



Role of hole transport layers in normal and inverted bulk heterojunction organic solar cells: A light intensity dependent capacitance-voltage analysis

Shailendra Kumar Gupta ^{a,*¹}, Durgesh C. Tripathi ^{b,1}, Amit Kumar ^c, Neha Garg ^d, Chinmay K. Gupta ^e, Vandana Yadav ^a, Sandeep Sharma ^a, Sanjeev Kumar ^f, Ashish Garg ^{g,h}

^a Amity School of Physical Sciences, Amity University Punjab, IT City, Sector 82A, Mohali, 140308, India

^b The Zisapel Nano Electronic Center, Department of Electrical Engineering, Technion-Israel Institute of Technology, Haifa, 32000, Israel

^c Clarendon Laboratory, Department of Physics, University of Oxford, Oxford, OX1 3PU, United Kingdom

^d Department of Computer Science and Engineering, Manav Rachna International Institute of Research and Studies, Faridabad, 121004, India

^e Department of Physics, National Post Graduate College, Barhalganj, 273402, Gorakhpur, India

^f Physics Department, Punjab Engineering College (Deemed to be University), Chandigarh, 160012, India

^g Department of Sustainable Energy Engineering, Indian Institute of Technology Kanpur, Kanpur, 208016, India

^h Chandrakanta Kesavan Center for Energy Policy and Climate Solutions, Indian Institute of Technology Kanpur, Kanpur, 208016, India



ARTICLE INFO

Keywords:
Bulk heterojunction
Capacitance-voltage
Surface photo-voltage
Carrier accumulation

ABSTRACT

In organic solar cells (OSC) hole transport layers (HTL) are essential for boosting the power conversion efficiency (PCE); therefore, it is crucial to determine the underlying mechanisms. In the present manuscript, we report a study that examines the effects of two HTL such as PEDOT:PSS and MoO₃, on the electrical characteristics of P3HT:PC₆₁BM (active layer) based bulk heterojunction (BHJ) in normal (ITO/PEDOT:PSS/P3HT:PCBM/Al) and inverted (ITO/ZnO/P3HT:PCBM/MoO₃/Ag) configurations. Current density-voltage (*J-V*) and illumination intensity dependent capacitance-voltage (*C-V*) measurements have been performed and compared for with and without HTL (PEDOT:PSS in normal and MoO₃ in inverted) devices. Results suggest that the extracted photovoltaic parameters (short circuit current density (J_{sc}), open circuit voltage (V_{oc}) and fill factor (FF)) of HTL containing devices are superior to without HTL devices in both normal and inverted OSC, due to unfavourable charge carrier accumulation and band bending in HTL free devices. Such charge build-up at active layer/anode interface generates photovoltage contributing as loss factor to PCE and has been investigated in *C-V* characteristics measured under varied illumination intensities (0/dark, 50 and 100 mWcm⁻²). Parameters such as built-in-voltage (V_{bi}), effective built-in-voltage ($V_{bi, eff}$), accumulated carrier concentration and surface photovoltage ($V_{SPV} = V_{bi, eff} - V_{bi}$) are extracted as a function of illumination intensity. Our findings reveal that HTL free devices, in both conventional and inverted OSCs structures, marked with low J_{sc} , V_{oc} and FF values generate higher SPV. The SPV calculation method used here has been proven to be crucial in recommending a suitable HTL for OSC device architectures.

1. Introduction

Power conversion efficiency and stability, two important aspects for successful commercialization of organic solar cells (OSC) are critically dependent on interfacial quality between the photo-absorbing active layer (polymer or small molecule) and top/bottom electrodes [1–5]. Most often, the quality of the interface is assured by the proper choice of interface materials either in the form of inorganic/organic thin films (solution processed/evaporated/nano particles) deposited either over

transparent conducting oxide (ITO) or below the top metal electrode often termed as buffer layers (BL), charge transport layers (CTL) or charge selective layers (CSL) [6–10]. These layers accomplish various complex functions such as matching of energy levels, determining device polarity, prohibiting physical/chemical reactions, and defect passivation in order to provide ohmic path to the photo-generated charges by reducing the interfacial energy barrier, leading to high charge collection efficiencies at the electrodes and hence crucial for PCE improvement [11–15]. Depending on their work functions, these layers

* Corresponding author.

E-mail address: shailendragupta5@gmail.com (S.K. Gupta).

¹ Authors have contributed equally to the work.

select photo-generated holes (PEDOT: PSS, MoO_x) or electrons (ZnO , TiO_2) for directed flow of charges towards ITO, resulting in varying device polarity in each case. A number of alternative HTL, including carbon-based (Carbon Nanotubes (CNTs) and Graphene, carbon black/paste), hydrophobic poly (triarylamine) (PTAA), PEDOT:PSS coupled with oxides and polymers, MXenes and self-assembled monolayers, have been created in addition to these well-established HTL to improve device PCE, stability, flexibility and cost effectiveness [16–20].

On the basis of polarity variation due to buffer layers, two different device configurations of opposite polarity (i) normal (ITO/PEDOT:PSS/Active layer/Al) and (ii) inverted (ITO/ZnO/Active layer/ MoO_3/Ag) OSCs have been realized [21]. OSCs with inverted configuration typically exhibit superior ambient stability in contrast to normal configuration due to the presence of stable metal electrodes, interfaces, and energetically favorable bulk heterojunction (BHJ) blend segregation [21–23]. The criteria of selection of these HTL and ETL should be determined based on their ability to transport selected charges, block unwanted carrier transport, and match energy levels with photo-active layer. ETL in inverted OSC, should have high transparency, electron mobility and stability. ETL should assist in transporting electrons towards cathode whilst blocking holes. However, HTL should assist in making an energetically favorable contact with active layer and improves the extraction of photo generated holes towards anode [24–26].

In addition to charge selection, these CSIs have been proved extremely successful in facilitating charge transport providing appropriate electric field distribution, polaron dissociation, exciton blocking, charge injection/extraction under device operation conditions impacting PCE [25,27,28]. Specifically, an efficient HTL should have both excellent electron blocking as well as hole extraction property. However, in HTL free, PV devices, there are always barrier to the charge extraction under illumination due to limited energy level matching between the active layer and metal electrode. Hence, such non-ideal contacts limits the spontaneous transport of photogenerated charge carriers leading to charge build up or accumulation at active layer/metal interface. Such charge accumulation induces unfavourable recombination and band bending, further decaying the PV parameters [11,29].

In the investigation of the role of HTL, majority of the literature offers a fair qualitative insight and hence a quantitative investigations are needed to understand the role of HTL in determining the device parameters such as interfacial energy barrier, electron/hole density (n/p), built-in potential/electric field (V_{bi}), open circuit voltage (V_{oc}) and mobility (μ) to realize a better planner and bulk heterojunction device design. Current density (J)- voltage (V), kelvin probe atomic force microscopy (KPFM), photoelectron spectroscopy (PES), and impedance spectroscopy (IS) have been used to electrically evaluate these contact-related issues in OSC [30,31], [32]. Among these, steady state capacitance-voltage ($C-V$) and capacitance-frequency ($C-f$) measurements under dark/illumination have been adopted extensively in organic and perovskite photovoltaic diodes to investigate the charge transport under dark and illumination in order to calculate device parameters such as built in voltage (V_{bi}), effective built in voltage ($V_{bi,eff}$), doping/defect density, carrier life time, mobility, bulk/interfacial charge accumulation density, Schottky barrier, electrical polarization, contact surface voltage, interfacial energy level alignment, degradation of contacts, contribution of traps, recombination mechanism and in assessing the width of density of states curve etc. [33–37].

$C-V$ characteristics, in such diodes are attained by scanning from reverse to forward bias, comprise of different regions with voltage. When the applied bias voltage is less than the threshold voltage for charge injection, no charges are injected from the injecting contacts and capacitance is nearly voltage independent from reverse bias to low forward voltage range signifying the active layer thickness called geometric capacitance (C_{geom}), then rises, with bias and in the moderate voltage range reaches to a maximum value (C_{max}) at a particular forward bias (V_{peak}) before falling [38,39]. For single carrier devices, C_{max} has been found to approach to the 3/4th of the C_{geom} in the space charge

limited (SCL) regime [40–42]. Prior to the peak, the voltage dependence of capacitance in C-V curves has been explained by Mott-Schottky (MS) relation by analyzing $1/C^2 - V$ data, however It is now widely acknowledged that the basic assumption used to generate the MS equation would not be suitable for analyzing the space charge limited (SCL) organic diodes [43,44]. Besides, a great deal of work has been done to comprehend the underlying physics on the occurrence of peak in the low-frequency $C-V$ curves of organic diode [45]. Mensfoort and Coehoorn proposed the participation of carrier diffusion and drift to the current density and recommended an empirical correlation between V_{bi} and V_{peak} in $C-V$ curve for the assessment of injection barriers [40,46,47]. Accordingly, above the threshold voltage under forward bias, charges are started to inject and concentration of injected charges increases with voltage followed by their diffusion and accumulation into the bulk with increasing applied voltage, resulting in an increase in the capacitance until built in potential (V_{bi}). Tripathi and Mohapatra further suggested that the $C-V$ peak originates due to the competition between the diffusive and drift transport of injected charge carriers and established a linear correlation between the diffusive capacitance ($C^{-2/3}$) and voltage (V) in diffusion-dominated regime [41]. Nonetheless, the usefulness of the drift-diffusion (D-D) based expression for the BHJ solar cells has been demonstrated in the literature, and the pertinent parameters, including built in voltage (V_{bi}) and surface photovoltage (SPV) under illuminations have been effectively extracted [33,38]. Above V_{bi} the occurrence of negative capacitance is also reported under unipolar and bipolar charge injection due to several reasons explained in the literature [34,48,49]. The observed peak in $C-V$ measurements has been investigated in literature extensively to understand sensitive changes in the charge transport primarily corresponds to theoretical V_{bi} [50]. The presence of more than one peak corresponds to the defects due to certain reasons such as contamination, doping and degradation phenomenon in the device [51].

In contrast to the dark measurements, J-V and C-V measurements of organic diodes in both fullerene (P3HT: PC₆₁BM, PTB7: PC₇₁BM) and non fullerene (PM6:Y6) BHJ, play a significant role under varied illumination intensity using neutral density filters. Light intensity dependent J-V signifies the recombination mechanism (J_{sc} Vs Light intensity) and ideality factor (V_{oc} Vs Light intensity). C-V characteristics with varied illumination intensity has been employed to measure surface charge accumulation and SPV in different-different cases such as annealed/unannealed active layer and in investigating the buffer layers [35,38,52–56]. The majority of the literature on light intensity dependent C-V is related to fullerene based BHJ systems and hardly covers the non-fullerene based OSC devices.

Since, $C-V$ characteristics, under illumination often gives an idea of photogenerated charge transport and the curve $\left(\frac{dC}{dV}\right)^{-2/5}$ Vs V is fitted linearly to determine voltage axis intercept, giving rise to effective built in voltage ($V_{bi, eff}$) at fixed illumination intensity [38]. The difference between calculated V_{bi} under dark and $V_{bi, eff}$ under illumination defines as surface photo-voltage (SPV) at that illumination intensity [26,33,38,57]. The main source of SPV has been suggested to be inevitable charge carrier accumulation at BHJ/electrode interface during transport to the respective electrodes which is supposed to be a primary loss factor to open circuit voltage (V_{oc}) and hence SPV is one of the important factors in determining the deviation in V_{oc} caused by band bending, originated due to charge accumulation or due to several other reasons [58]. Inferior interface quality due to misalignment in energy levels, could be one of the important factors in case of without HTL devices that leads to a significant accumulation of photo generated charges at the absorber/electrode interfaces [59,60]. Hence calculations of SPV would be beneficial in comparative understanding of charge accumulation in with and without HTL OSC devices to understand the loss in V_{oc} and hence in PCE. Such comparative studies involving the determination of SPV in with and without HTL devices, signifying the role of HTL in OSCs have

not been published so far to the best of our knowledge and hence an attempt has been made in the following sections.

Here, in the present manuscript we have measured *SPV* for normal and inverted device configurations fabricated with and without HTL (in normal **PEDOT: PSS** and in inverted **MoO₃**) based on the active layer blend of P3HT: PCBM (Poly 3-hexylthiophene (P3HT): (6, 6) phenyl C61 butyric acid methyl ester (PC₆₁BM)), a reliable system with well documented device information. Further, their *C-V* measurements were conducted under dark and variable light intensity to calculate V_{bi} and $V_{bi, eff}$, *SPV* and carrier concentration signifying the role of HTL.

2. Experimental details

To investigate the impact of HTL, such as PEDOT: PSS in normal OSC (ITO/PEDOT: PSS/P3HT: PCBM/Al) and MoO₃ in inverted OSC (ITO/ZnO/P3HT: PCBM/MoO₃/Ag) configurations, devices were fabricated as with and without HTL as shown schematically in Fig. 1 (a and c) with their respective energy band diagrams (b and d). Energy band diagram also reflects the selection criteria of PEDOT:PSS in normal OSC and ZnO/MoO₃ combination in inverted devices due to their energy levels matching with P3HT: PCBM active layer to provide ohmic contact to selected photo generated charges. In inverted devices ZnO has been used as an electron transport layer (ETL) layer that helps in inverting the charge transport (device polarity) in comparison to normal configuration. Both normal and inverted devices were fabricated over pre-patterned Indium Tin oxide coated glass (ITO/Glass) substrates. ITO/Glass were initially cleaned in a boiling soap solution for 15 min, followed by rinsing 3 times in DI water. Later ITO/Glass were ultrasonicated in acetone and isopropyl alcohol (IPA) 10 min each followed by drying using N₂ gas. Thereafter, substrates were UV ozone treated for 20 min, prior to CSLs deposition to reduce ITO surface roughness and increasing its surface energy by removing carbon based contamination of the surface.

To fabricate normal OSC, HTL of PEDOT: PSS (dissolved in DI water in 1:2 ratios) was spin coated at 2000 rpm/60 s on the pre ozonized ITO/Glass substrates and thermally dried at 150 °C for 10 min on a hot plate

in air to yield a 35 nm thick film. To fabricate inverted devices, first the ETL of ZnO layer was fabricated from a solution of 0.45 M concentration, prepared after mixing zinc acetate di hydrate (C₄H₁₀O₆Zn), 2-methoxy ethanol (C₃H₈O₂) and ethanolamine (C₂H₇NO). Prepared solution was spin casted at 2000 rpm/60s on pre-ozonized ITO/Glass substrates followed by annealing at hot plate in air at 250 °C for 10 min to yield 30 nm thin ZnO film. ETL and HTL coated (ZnO/ITO/Glass, PEDOT: PSS/ITO/Glass) and few bare ozonized ITO/Glass (for without PEDOT: PSS devices) were transferred in to N₂ filled glove box to spin coat P3HT: PCBM (w/w 1:0.8 in 1 ml chlorobenzene) active layer solution at 1500 rpm/60s. Coated, wet P3HT: PCBM films were thermally annealed at 150 °C for 10 min in the glove box to form ~80–90 nm thick nano scale morphology with optimum absorbance. From here (i) P3HT: PCBM/ITO/Glass, (ii) P3HT: PCBM/PEDOT: PSS/ITO/Glass and (iii) P3HT: PCBM/ZnO/ITO/Glass substrates were transferred into thermal evaporator to deposit Al (100 nm) on (i) and (ii) and MoO₃ (0 and 10 nm)/Ag (100 nm) on (iii) by using shadow masks at 0.5 Å/s deposition rate at 5 × 10⁻⁶ mbar. Finally, the following device configurations were received from thermal evaporator (A) ITO/P3HT: PCBM/Al (B) ITO/PEDOT: PSS/P3HT: PCBM/Al (C) ITO/ZnO/P3HT: PCBM//Ag and (D) ITO/ZnO/P3HT: PCBM/MoO₃/Ag. The detailed procedure adopted here, can be found out elsewhere [25]. In each case (A-D) 4 different devices have been characterized to ensure reproducibility. The devices with area 0.09 cm² were characterized under 1 sun illumination calibrated on a Newport solar simulator using Keithley 2400 source meter for *J-V* measurements under unencapsulated condition. *C-V* characteristics were performed under dark and varied illumination using Agilent 4294 A Precision Impedance Analyzer at an A.C. voltage of 50 mV (rms). Variation in illumination intensity was performed by using the neutral density filters. The thickness of the stacking layers (HTL/ETL/active layer) were determined using the styles based profilometer.

3. Results and discussion

OSC devices were fabricated in four different configurations as A (normal OSC without PEDOT: PSS), B (normal OSC with PEDOT: PSS), C

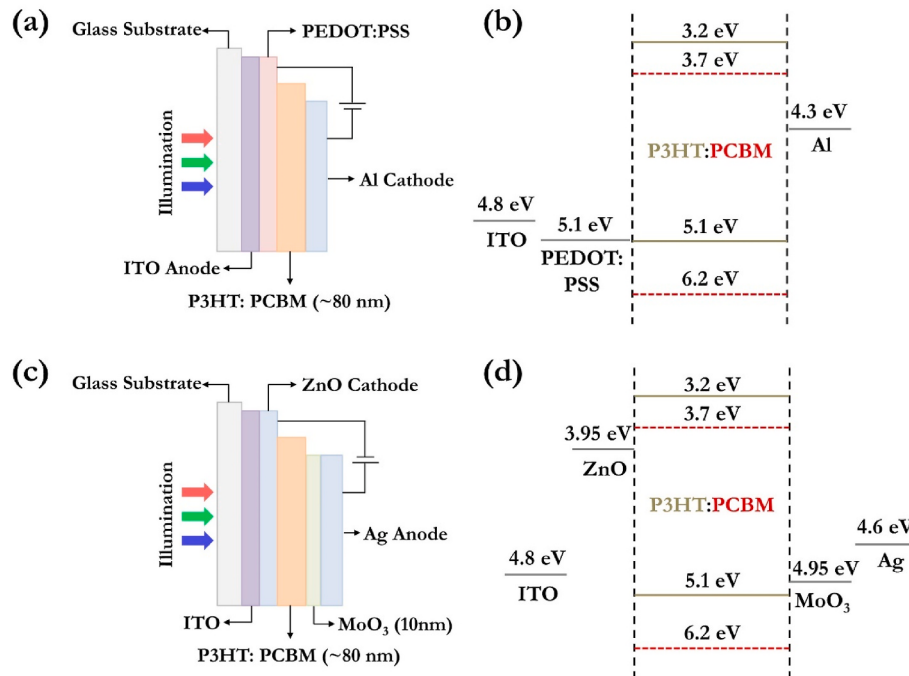


Fig. 1. Schematic of (a) normal OSC configuration (b) corresponding energy level diagram, (c) Inverted OSC configuration and (d) corresponding energy level diagram. The hole transport layers (HTL), PEDOT: PSS in the normal and MoO₃ in the inverted OSC, are further removed to investigate its impact on the electrical characteristics.

(inverted OSC without MoO₃) and D (inverted OSC with MoO₃). The corresponding J-V and C-V characteristics have been investigated under dark and illuminations in the following sections.

3.1. J-V characteristics under illumination and dark

The illuminated and dark J-V characteristics for normal (PEDOT: PSS/Al) and inverted configuration (ZnO/MoO₃), with and without HTL (PEDOT: PSS and MoO₃) were measured for above mentioned A, B, C and D configurations and results are depicted in Fig. 2(a-d). The extracted, short circuit current density (J_{sc}), open circuit voltage (V_{oc}), Fill factor (FF), series resistance (R_s), shunt resistance (R_{sh}) and PCE have been summarized in Table 1. Here, it is evident that the devices comprising of HTL (PEDOT: PSS and MoO₃), irrespective of normal or inverted, attain high PCE in comparison to without HTL devices. The absence of HTL leads to a significant drop in PV parameters J_{sc} , V_{oc} , FF and PCE. Normal OSC, with PEDOT: PSS contributes maximum J_{sc} of 9.76 mAcm⁻², V_{oc} of 0.62 V and FF of 0.58 and are reduced to J_{sc} of 8.15 mAcm⁻², V_{oc} of 0.52 V and FF of 0.49 for normal OSC without PEDOT: PSS and hence PCE of 3.60 % and 2.07 % are observed for with and without HTL (PEDOT: PSS). Similarly, in inverted OSC devices with MoO₃ (HTL) perform significantly better than without MoO₃. Inverted OSC with MoO₃ contributes to J_{sc} of 9.19 mAcm⁻², V_{oc} of 0.64 V and FF of 0.57 that are further reduced to J_{sc} of 6.67 mAcm⁻², V_{oc} of 0.58 V and FF of 0.45 for without MoO₃ buffer layer and hence PCE of 3.04 % and 1.70 % have been observed for with and without HTL (MoO₃) in inverted configuration. The PCE values observed above are similar to the reported values for P3HT: PCBM blend system [61]. While comparing the performance of normal and inverted OSC (A and D), the performance of normal OSC devices has been found slightly better than inverted devices, contrary to the published reports in literature where inverted OSC are performing better than normal OSC devices due to improvement in short circuit current density (J_{sc}) [62]. However, improved normal devices is possibly due to 10 nm thick additional MoO₃ buffer layer causing enhanced series resistance in inverted devices. However, the stability

Table 1

Performance of normal and inverted OSC devices with and without hole transport layer in terms of short circuit current density (J_{sc}), open circuit voltage (V_{oc}), Fill factor (FF), series resistance (R_s), shunt resistance (R_{sh}) and Power conversion efficiency (η).

Device specification	J_{sc} (mAcm ⁻²)	V_{oc} (Volt)	FF	R_s (Ωcm^2)	R_{sh} (Ωcm^2)	PCE (%)
Normal with PEDOT: PSS	9.76	0.62	0.58	9.3	820	3.60
Normal without PEDOT: PSS	8.15	0.52	0.49	18.4	782	2.07
Inverted with MoO ₃	9.19	0.64	0.57	10.4	625	3.04
Inverted without MoO ₃	6.67	0.58	0.45	29.2	346	1.70

performance of inverted OSC device is far better than normal OSC device, which is the only benchmark for evaluating the performance variations which we have shown in our previously published works [36].

Besides, no S shaped curve has been observed in any without HTL devices. The corresponding dark J-V curves have been depicted in Fig. 2 (b and d) in log-log scale. As evident in both configurations, leakage currents have been greatly suppressed, however high diffusion SCLC currents are observed in the forward region leading to improved rectification ratio $\frac{J_{forward}}{J_{reverse}}$ in with HTL devices i.e. higher injection current and lower leakage have improved the device performance. Low diffusion currents for without HTL devices show insulating character of the interfaces. Decreasing reverse current densities for standard devices clearly demonstrate the role of HTL in suppressing the electron injection from the metal electrode as well as from ITO. In the intermediate voltages the slope of the exponential regime is always higher for with HTL devices and hence achieves better ideality factor for standard devices. At higher voltage, dark current is limited by R_s and hence significantly reduced current densities are observed for without HTL device, which is

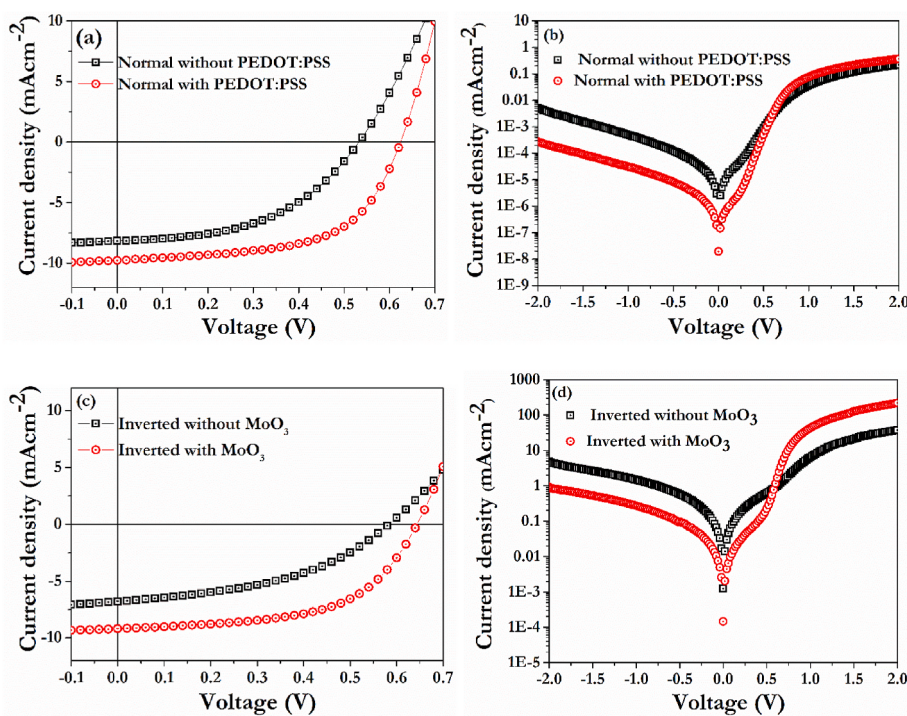


Fig. 2. J-V characteristics (a) under illumination and (b) under dark for normal OSC devices with architectures ITO/PEDOT: PSS/P3HT: PCBM/Al (with PEDOT: PSS) and ITO/P3HT: PCBM/Al (without PEDOT: PSS) and (c) under illumination and (d) under dark for inverted OSC devices with architectures ITO/ZnO/P3HT: PCBM/MoO₃/Ag (with MoO₃) and ITO/ZnO/P3HT: PCBM/Ag (without MoO₃).

also consistent with Table 1.

3.2. Capacitance - voltage (C-V) characteristics

To understand the behavior of injected and photo generated charge carriers under applied bias, C-V measurements under varying illumination intensities (0/dark, 50 and 100 mWcm⁻²) have been performed on both normal and inverted OSC with and without HTL (A, B, C and D) configurations. The measured C-V characteristics at 1 kHz modulation frequency provide an understanding on photovoltaic and charge accumulation under varied device structure (with and without HTL) and illumination intensities. The observations and analysis of C-V characteristics to determine built in voltage (V_{bi}), effective built-in potential ($V_{bi, eff}$), surface photo voltage (SPV) and carrier concentration are discussed in the following sections.

3.2.1. Normal OSC devices: with and without HTL (PEDOT: PSS)

The C-V characteristics of ITO/PEDOT: PSS/P3HT: PCBM/Al and ITO/P3HT: PCBM/Al devices (with and without PEDOT: PSS) are shown in Fig. 3 (a and b). The obtained C-V characteristics follow the important regions of charge depletion, accumulation, and recombination along with a characteristic peak (V_{peak}) while scanned from reverse to forward biasing. Evidently V_{peak} , indicating maximum capacitance (C_{max}), has been very successful in determining the photo induced charge accumulation in double charge carrier organic diodes. Relative increase or decrease in V_{peak} corresponds to less and more interfacial accumulation at electrode interfaces respectively [53,63]. The observed V_{peak} here, is directly related to the built-in-voltage (V_{bi}) in the device but does not determine it accurately, however, is significant in understanding the role of energy barrier at BHJ/electrodes.

As evident, under dark conditions the V_{peak} corresponding to C_{max} are found to be located at 0.62 and 0.46 V for with and without PEDOT: PSS HTL respectively, suggesting an increased energetic barrier at ITO in the absence of PEDOT: PSS, leading to reduced carrier injection; and hence significant reduction has been observed in C_{max} due to appreciable charge injection in PEDOT: PSS devices. The reverse/geometric capacitance (C_{geom}) measured at -1.0 V has been found to be higher (4.36 nF) for with PEDOT: PSS device in comparison to without PEDOT: PSS device (3.25 nF) even though the thickness of the active layer and device area have been kept identical. Additional contribution to C_{geom} , under dark in case of with PEDOT: PSS devices may be originated due to the charging of interfacial states located at hetero interface of donor (P3HT) and acceptor (PCBM) molecules in photoactive layers [64].

Under varied illumination, the obtained C-V curves follow the same

pattern as in the dark, starting from saturated capacitance under deep reverse bias, voltage dependent capacitance increasing up to V_{peak} and then decreases to a saturated value in the deep forward bias. Here, externally applied field helps against V_{bi} of the device in transporting the photogenerated charges towards top and bottom electrodes and gets accumulated at the electrodes depending on interfacial energetics. Increase in illumination intensity (50 and 100 mWcm⁻²) shifts the V_{peak} towards lower bias voltage, suggesting increased charge accumulation with increasing illumination as density of charge carriers increase with illumination. However, more intense peaks (increased C_{max}) have been observed with increase in illumination intensity in comparison to dark condition. Shift in V_{peak} with varied illumination is found to be more significant in without PEDOT: PSS devices and a significant increase in C_{max} for without PEDOT: PSS has been observed. At 100 mWcm⁻² illumination intensity, the C-V peak is observed at 0.52 V and 0.32 V for with and without PEDOT: PSS devices, respectively and hence an increased shift in V_{peak} ($\Delta V_{peak} \sim 100$ mV) has been observed for without PEDOT: PSS devices, depicting more charge accumulation of photo generated charges at the interface in comparison to with PEDOT: PSS devices ($\Delta V_{peak} \sim 20$ mV). Which is evident in light J-V parameters in Table 1, indicating suppressed V_{oc} and FF in without PEDOT: PSS devices due to interfacial accumulation. Besides, the reverse capacitance increases remarkably compared to the dark condition. It is evident that the capacitance under illumination follows a voltage dependent trend at deep reverse bias. Under reverse bias, in between -1.0 and 0.5 V broad shoulders have been observed with enhanced values of capacitances under photo excitation for with PEDOT: PSS devices. Similar, occurrence has been identified as bulk polarization in case of perovskites solar cells due to its ionic nature possibly due to the ionic nature of PEDOT: PSS, contributing to capacitance under illumination as such C-V trends are absent in PEDOT: PSS free and inverted devices [65]. Following, we will investigate the C-V curves for inverted OSC consisting of similar P3HT: PCBM active layer under illumination in comparison to the normal structure.

3.2.2. Inverted OSC devices: with and without HTL (MoO₃)

The C-V characteristics of inverted OSC with and without MoO₃ HTL measured are displayed in Fig. 4a and b, for three different illumination intensities (0/dark, 50 and 100 mWcm⁻²). Under the dark condition, C_{geom} is found to be voltage independent for both inverted OSC with and without MoO₃ even under increasing illumination intensities and corresponds to the thickness of P3HT: PCBM active layer hence an entirely different illumination response of C-V characteristics under reverse bias operation have been observed for inverted OSC in comparison to normal

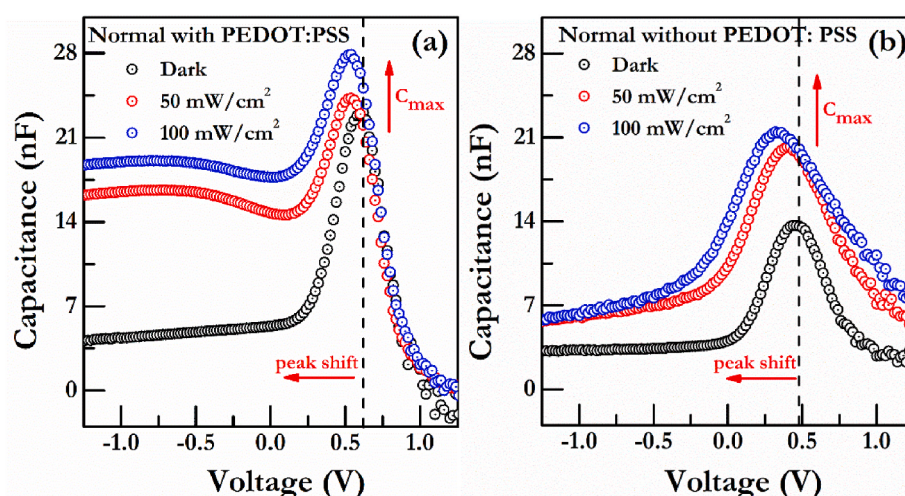


Fig. 3. C-V characteristics of normal BHJ solar cells at three different illumination intensities (a) with buffer layer and (b) without buffer layer. Note that the capacitance value in the reverse bias as well as around the peak voltage changes significantly with illumination intensity.

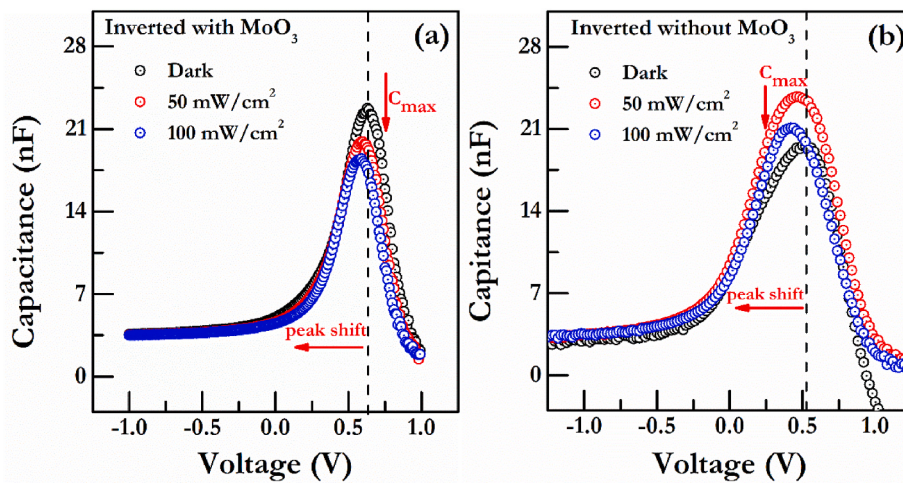


Fig. 4. C-V characteristics of inverted BHJ solar cells at three different illumination intensities (a) with buffer layer and (b) without buffer layer. Note that the capacitance value in the reverse bias remains almost constant with voltage and intensity variation however, it changes noticeably around the peak voltage.

OSC.

As evident, under dark, V_{peak} in the C-V curve has occurred at 0.68 V and 0.52 V for with and without MoO_3 , thus 0.16 V shift suggests increased anode energy barrier leading to lower capacitance due to less charge injection for without MoO_3 devices. Under illumination, V_{peak} is again found to be shifted towards the lower bias in both cases, however capacitance is found to be increase in without MoO_3 devices suggesting decreased charge extraction efficiency in without MoO_3 . Furthermore, the shift in V_{peak} (ΔV_{peak}) for varied illumination ($10\text{--}100 \text{ mW cm}^{-2}$) is larger for without MoO_3 ($\Delta V_{peak} \sim 80 \text{ mV}$) in comparison with MoO_3 device ($\Delta V_{peak} \sim 50 \text{ mV}$). Although C_{max} of inverted OSC indeed shows illumination intensity dependence, as with MoO_3 inverted OSC device, depicts a monotonous decrease with increasing illumination from dark (0 mW cm^{-2} to 100 mW cm^{-2}). However, without MoO_3 layer C_{max} shows non-monotonic dependence. For without MoO_3 devices, C_{max} values for 50 and 100 mW cm^{-2} are always less than the dark C_{max} value. Furthermore, observation of illumination intensity independent reverse bias capacitance of inverted solar cells gives us an opportunity to critically analyze the variation of low-frequency C-V peak height under illuminations.

3.3. Determination of surface photo voltage (SPV)

Since, MS equation has been found inappropriate in analyzing C-V characteristics of space charge limited (SCL) organic diodes due to underlying assumptions, we have incorporated an analytical model given by Tripathy and Mohapatra based on D-D model by taking into account additional carriers stored under the carrier profile with applied voltage to understand the diffusive capacitance (C_{diff}) prior to peak voltage which leads to a linear voltage relationship $C_{diff}^{-2/3} \alpha (V - V_{bi})$ [41]. Usually, C_{diff} from the measured C-V, is obtained by subtracting C_{geom} , corresponds to geometrical thickness. Later, Upkaret *et al.* showed that the robustness of this model can be improved by incorporating the derivative of capacitance with voltage to eliminate voltage independent contribution to measured capacitance leading to following expression [38].

$$\frac{dC_{meas}}{dV} = \frac{dC_{diff}}{dV} = -\frac{3qAp_0d}{4} \left(\frac{k_B T}{q} \right)^{1/2} (V - V_{bi})^{-5/2} \quad 1$$

here, q is the elementary charge, A is the area, d is the active layer thickness, p_0 is the carrier concentration at injecting electrodes. This expression predicts $\left(\frac{dC_{meas}}{dV} \right)^{-2/5}$ Vs V plot is linear, and the slope of this

plot represents carrier concentration at electrode, while voltage axis intercept determines V_{bi} . Following, We use this method to describe the C-V curves for with and without HTL in both normal and inverted OSCs under dark and varied illumination.

Fig. 5a and b, shows the $\left(\frac{dC_{meas}}{dV} \right)^{-2/5}$ Vs $(V - V_{bi})$ plots of normal OSC

with and without PEDOT: PSS layers for varying illumination intensity derived from **Fig. 3a** and **b**. Indeed, a linear regime can be identified in the wider voltage range at all illumination intensities, and is fitted excellently with a straight line to determine voltage axis intercept and the slope for both structures. Under the dark condition, the voltage axis intercept is found to be equal to 0.70 V and 0.64 V for with and without PEDOT: PSS anode buffer layer samples, respectively. The intercept voltage under dark condition is usually very close to the theoretical V_{bi} and it is attributed as onset voltage for the SCL injection. Increase in the onset voltage with insertion of PEDOT: PSS clearly indicates that reduction of injection barrier at anode contact, results in remarkable improvement in the V_{bi} is noted. The value of carrier concentration at injecting electrodes has been determined from the slope using Eq. (1).

The voltage-axis intercept of linear fitting of $\left(\frac{dC_{meas}}{dV} \right)^{-2/5} \alpha (V - V_{bi})$ plots show illumination intensity dependence, and it is always greater than the dark condition for both structures. Furthermore, the slope of this fitting decreases monotonically with illumination intensity. The voltage axis intercept under illumination yields the effective built-in voltage ($V_{bi,eff}$) at a given illumination intensity and slope determines the carrier concentration at injecting electrode as a function of illumination intensity. The calculated values of effective built-in voltage ($V_{bi,eff}$) and the accumulated carrier concentration are shown as a function of illumination intensity in **Fig. 5(c)** and **(d)**. Evidently, the $V_{bi,eff}$ and the accumulated carrier concentration increase monotonically with illumination intensity for both with and without HTL devices in normal configuration.

Similarly, $\left(\frac{dC_{meas}}{dV} \right)^{-2/5} \alpha (V - V_{bi})$ plots of inverted OSC with and without MoO_3 for varying illumination intensities are displayed in **Fig. 6a** and **b** and the linear regime identified at all illumination intensities are fitted excellently with a straight line for both with and without MoO_3 devices. The voltage axis intercept under dark condition is found to equal to 0.74 V for with buffer layer and 0.45 for without buffer layer samples. The intercept voltage under dark condition is very close to the theoretical V_{bi} and attributed as onset voltage for SCL injection. Increase in onset voltage with introducing of anode buffer layer clearly demonstrates the reduction of injection barrier height at anode contact, as a

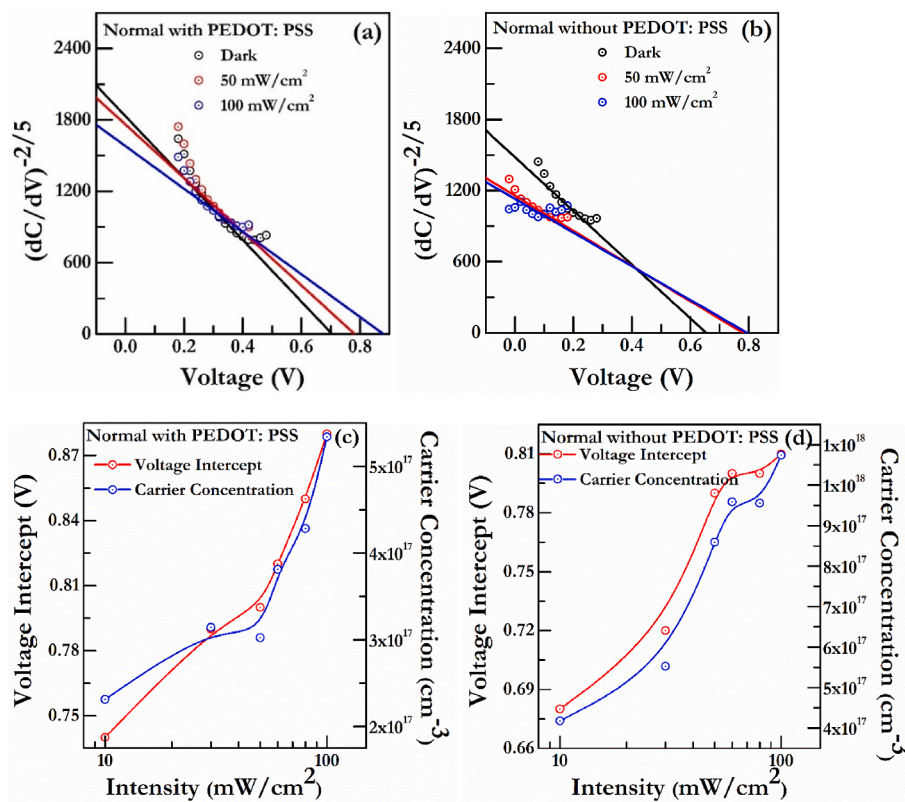


Fig. 5. $(dC/dV)^{-2/5}$ vs. V curves of normal BHJ solar cells at three different illumination intensities with PEDOT: PSS layer (a) and without PEDOT: PSS layer(b). Note that a linear regime is observed for both structures at all intensities. (c-d) The intercept-voltage and carrier concentration at injecting electrodes, obtained by linearly fitting the $(dC/dV)^{-2/5}$ vs. V curves with (c) and without (d) PEDOT: PSS as a function of illumination intensity.

result in remarkable improvement in the V_{bi} is noted. The value of carrier concentration at injecting electrodes determined from the slope using Eq. (1) and it is found to be very close for both inverted structures.

The voltage-axis intercept of linear fitting of $\left(\frac{dC_{meas}}{dV}\right)^{-2/5} \alpha (V - V_{bi})$ plots show illumination intensity dependence, and it is always greater than the dark condition for both structures. Furthermore, the slope of this fitting decreases monotonically with illumination intensity.

Illumination intensity dependence voltage axis intercept and the accumulated carrier concentration derived from the slope of $\left(\frac{dC_{meas}}{dV}\right)^{-2/5} \alpha (V - V_{bi})$ plot using Eq. (1) are shown as a function of illumination intensity in Fig. 6(c) and (d). Evidently, the $V_{bi,eff}$ and the accumulated carrier concentration increases monotonically with illumination intensity for both structures. Furthermore, the change of $V_{bi,eff}$ and the accumulated carrier concentration with respect to dark condition is found to be greater for the samples which has not consisted of anode buffer layer.

The difference of built-in voltages under dark (V_{bi}) and under illumination ($V_{bi,eff}$) and measures ($\Delta V_c = V_{bi,eff} - V_{bi}$) the surface photovoltage (SPV) at that particular illumination intensity and considered to be the bad bending at the interface due to charge accumulation under light. $V_{bi,eff} - V_{oc}$ is another way to calculate bend bending at Active layer and its interfaces in case of with and without HTL. Both $V_{bi,eff} - V_{bi}$ and $V_{bi,eff} - V_{oc}$ for normal and inverted configurations with and without HTL as a function of illumination are shown in Fig. 7. Clearly, band bending in case of with and without PEDOT: PSS is lying between 0.12–0.26 and 0.19–0.32 V respectively as a function of illumination. Slightly higher values for without PEDOT: PSS devices in comparison to with PEDOT: PSS devices at 100 mWcm^{-2} suggests reduced band bending in the presence of PEDOT: PSS. Similarly, in the presence of MoO_3 in inverted configuration observed ΔV_c is $\sim 0.18 \text{ V}$ at 100 mWcm^{-2} , which is lower

than 0.25 V in the absence of MoO_3 in the device. Hence, degradation in the performance of without MoO_3 device is due to contact related band bending. Over all the absence of HTL increases the band bending at contacts leading to decay in the performance in comparison to with HTL devices.

3.4. Energy band diagram

Energy band diagram for with and without HTL in normal and inverted devices has been depicted in Fig. 8 under dark condition. Clearly, the absence of HTL in both (normal and inverted) OSC devices enhances the barrier for hole transport between electrode/P3HT interface resulting in an improved build up of injected holes (accumulation). Presence of HTL (PEDOT:PSS and MoO_3) reduces charge accumulation. Similarly, photoinduced charge carriers can also accumulated at the interfaces generates a loss in V_{oc} and FF in without HTL devices.

4. Conclusions

In conclusion, the conventional PEDOT:PSS and ZnO/MoO_3 based inverted OSC (with and without HTL) comprising of P3HT: PCBM blend as an active layer, have been fabricated successfully. The devices have been electrically evaluated in terms of $J-V$ and $C-V$ characteristics under dark and varied illumination. Results suggest that HTL layer has a profound impact on PCE as HTL free devices in both normal and inverted configurations depict degraded $J-V$ performance due to excessive charge accumulation at interfaces as shown in Table 1. We have quantified surface photovoltage and charge accumulation by measuring the low frequency $C-V$ curves under dark and varied illumination intensities and exhibited a strong dependence of illumination intensity on the variations in $C-V$ curves for with and without HTL devices. Drift-diffusion model based analysis of light dependent $C-V$ curves have shown a

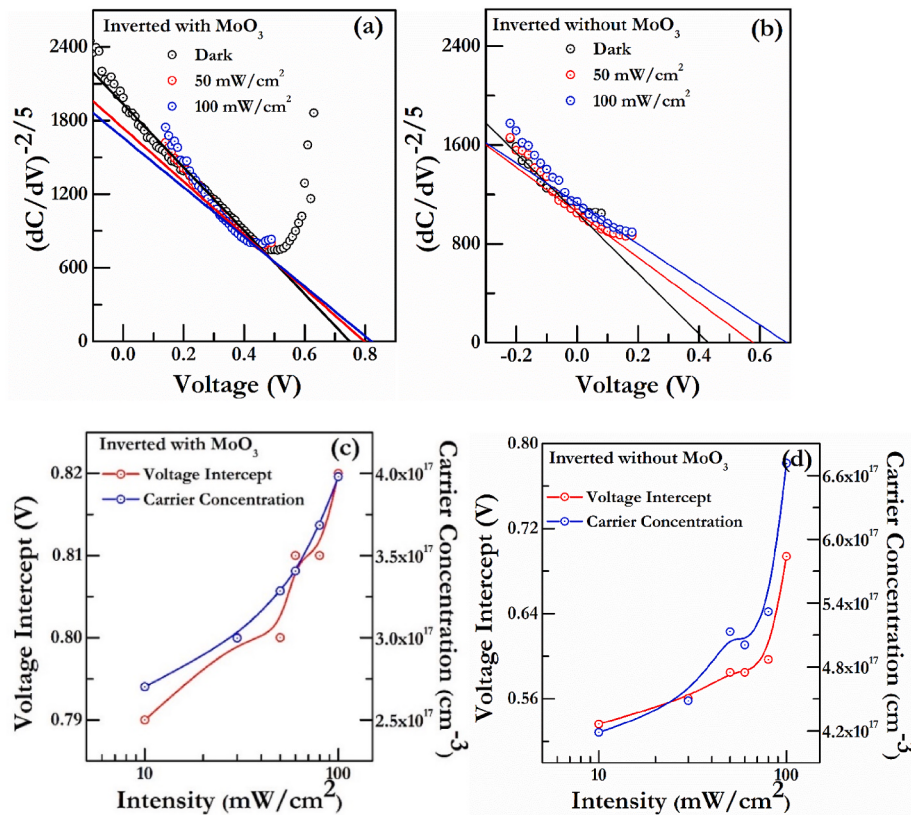


Fig. 6. $(dC/dV)^{-2/5}$ vs. V curves of inverted BHJ solar cells at three different illumination intensities (a) with and (b) without MoO_3 anode buffer layer. Note that a linear regime is observed for both structures at all intensities. (c-d) The intercept-voltage and carrier concentration at injecting electrodes, obtained by linearly fitting the $(dC/dV)^{-2/5}$ vs. V curves for with (c) and without MoO_3 devices, are plotted as a function of illumination intensity.

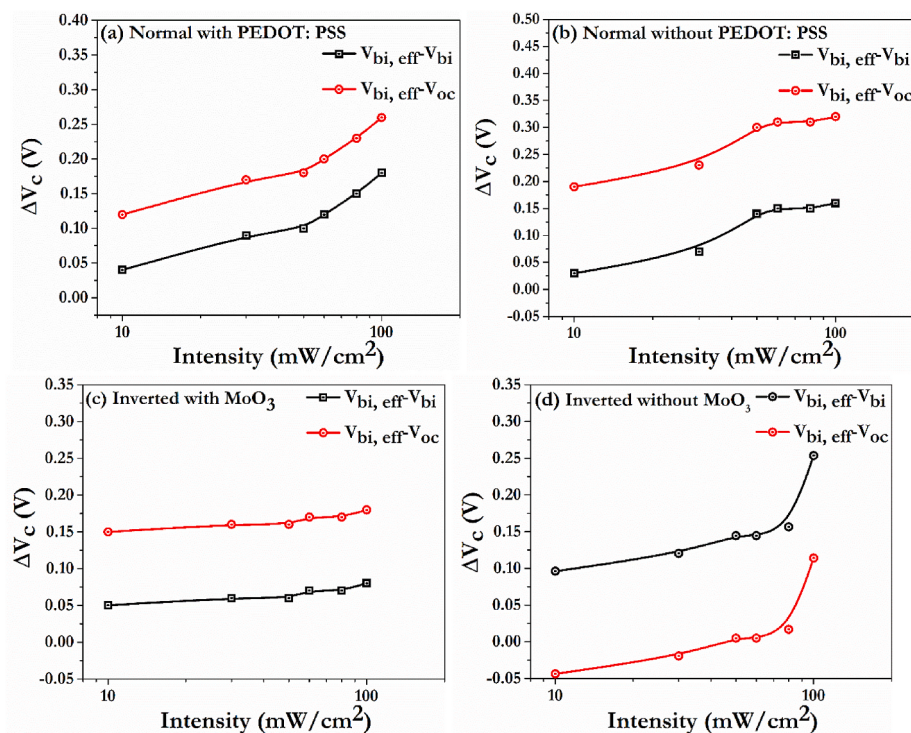


Fig. 7. The difference of effective built-in voltage with built-in voltage, and open circuit voltage as a function of illumination intensity for (a) ITO/PEDOT: PSS/ P3HT: PCBM/Al (with PEDOT: PSS) (b) ITO/P3HT: PCBM/Al (without PEDOT: PSS) (c) ITO/ZnO/P3HT: PCBM/ MoO_3 /Ag (d) ITO/ZnO/P3HT: PCBM/Ag (without MoO_3).

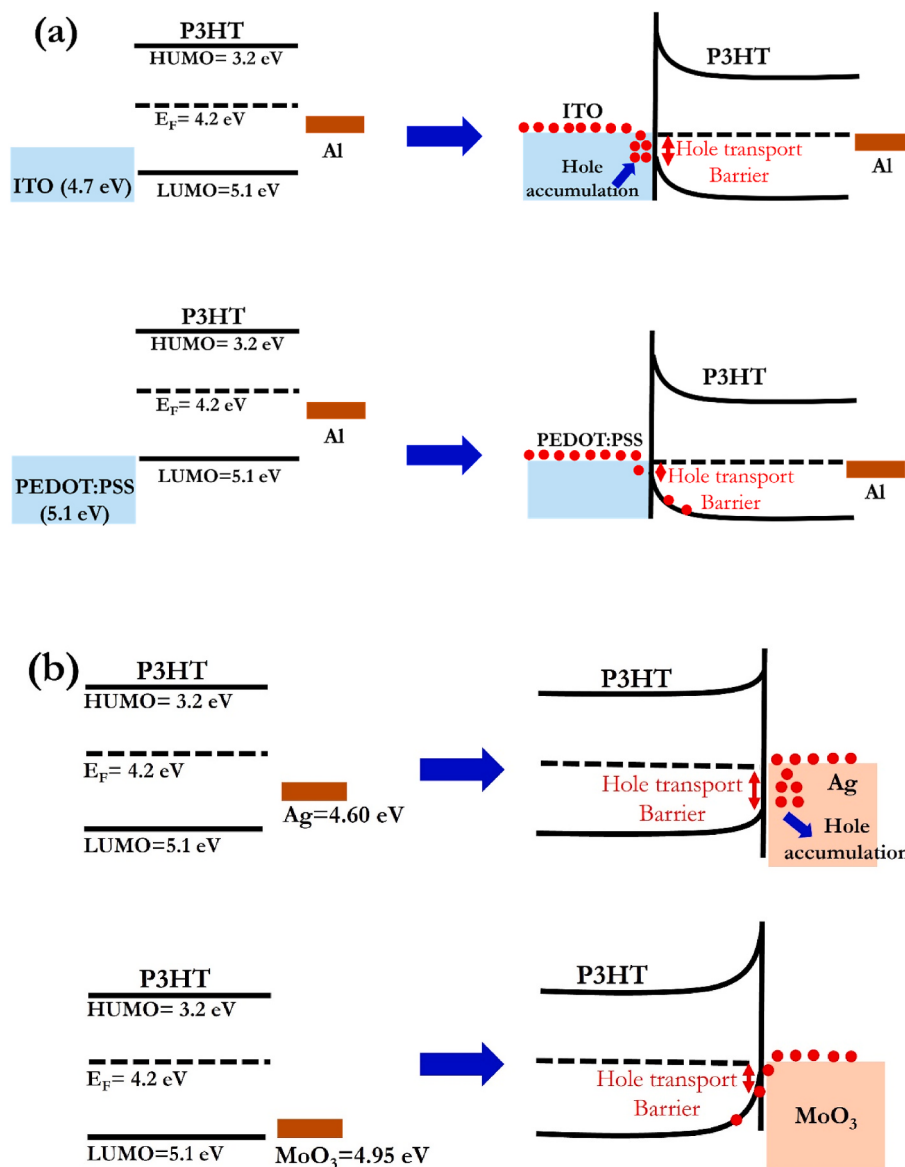


Fig. 8. Energy band diagram depicting the Active layer/HTL interface under dark (a) normal PEDOT:PSS/P3HT interface (ITO/P3HT/Al and PEDOT:PSS/P3HT/Al) (b) inverted P3HT/MoO₃ interface (P3HT/Ag and P3HT/MoO₃/Ag). Barrier to hole injection is four condition is shown and is responsible for charge accumulation.

strong dependence of $V_{bi, eff}$ on illumination intensity and hence surface photovoltage and carrier concentrations are calculated. Higher SPV and accumulated charge concentration have been observed in case of without HTL based normal and inverted OSC, which are playing an important contribution in reducing PCE in without HTL OSC. At 100 mWcm⁻² intensity, the observed SPV values and accumulated charge concentration for without HTL devices in normal and inverted devices are found to be 1.5 and 2 times more than the values observed for with HTL devices. This paper presents a strategy that may be used to analyze and isolate the impact of contacts to voltage loss in any optimization program or emerging technology.

CRediT authorship contribution statement

Shailendra Kumar Gupta: Writing – original draft, Methodology, Conceptualization. **Durgesh C. Tripathi:** Writing – review & editing, Supervision. **Amit Kumar:** Writing – review & editing. **Neha Garg:** Writing – review & editing. **Chinmay K. Gupta:** Writing – review & editing. **Vandana Yadav:** Writing – review & editing. **Sandeep Sharma:** Writing – review & editing. **Sanjeev Kumar:** Writing – review

& editing. **Ashish Garg:** Writing – review & editing, Supervision.

Declaration of competing interest

The authors declare that they have no known competing financial interests or personal relationships that could have appeared to influence the work reported in this paper.

Data availability

Data will be made available on request.

References

- [1] W. Yang, W. Wang, Y. Wang, R. Sun, J. Guo, H. Li, M. Shi, J. Guo, Y. Wu, T. Wang, G. Lu, C.J. Brabec, Y. Li, J. Min, Balancing the efficiency, stability, and cost potential for organic solar cells via a new figure of merit, Joule 5 (2021) 1209–1230, <https://doi.org/10.1016/j.joule.2021.03.014>.
- [2] S. Bi, X. Leng, Y. Li, Z. Zheng, X. Zhang, Y. Zhang, H. Zhou, Interfacial modification in organic and perovskite solar cells, Adv. Mater. 31 (2019) 1805708, <https://doi.org/10.1002/adma.201805708>.

- [3] H. Tang, Y. Bai, H. Zhao, X. Qin, Z. Hu, C. Zhou, F. Huang, Y. Cao, Interface engineering for highly efficient organic solar cells, *Adv. Mater.* n/a (2023) 2212236, <https://doi.org/10.1002/adma.202212236>.
- [4] L. Tian, Q. Xue, Z. Hu, F. Huang, Recent advances of interface engineering for non-fullerene organic solar cells, *Org. Electron.* 93 (2021) 106141, <https://doi.org/10.1016/j.orgel.2021.106141>.
- [5] A. Garg, S.K. Gupta, J.J. Jasieniak, T.B. Singh, S.E. Watkins, Improved lifetimes of organic solar cells with solution-processed molybdenum oxide anode-modifying layers, *Prog. Photovoltaics Res. Appl.* 23 (2015), <https://doi.org/10.1002/pip.2512>.
- [6] K. Wang, C. Liu, T. Meng, C. Yi, X. Gong, Inverted organic photovoltaic cells, *Chem. Soc. Rev.* 45 (2016) 2937–2975, <https://doi.org/10.1039/C5CS00831J>.
- [7] S. Bishnoi, R. Datt, S. Arya, S. Gupta, R. Gupta, W.C. Tsou, S.N. Sharma, S.P. Patole, V. Gupta, Engineered cathode buffer layers for highly efficient organic solar cells: a review, *Adv. Mater. Interfac.* 9 (2022) 2101693, <https://doi.org/10.1002/admi.202101693>.
- [8] S. Banerjee, S.K. Gupta, A. Singh, A. Garg, Buffer layers in inverted organic solar cells and their impact on the interface and device characteristics: an experimental and modeling analysis, *Org. Electron. Physics, Mater. Appl.* 37 (2016), <https://doi.org/10.1016/j.orgel.2016.06.031>.
- [9] S.K. Gupta, R. Jindal, A. Garg, Microscopic investigations into the effect of surface treatment of cathode and electron transport layer on the performance of inverted organic solar cells, *ACS Appl. Mater. Interfaces* 7 (2015), <https://doi.org/10.1021/acsami.5b03583>.
- [10] P. Schulz, J.O. Tiepelt, J.A. Christians, I. Levine, E. Edri, E.M. Sanehira, G. Hodes, D. Cahen, A. Kahn, High-work-function molybdenum oxide hole extraction contacts in hybrid organic-inorganic perovskite solar cells, *ACS Appl. Mater. Interfaces* 8 (2016) 31491–31499, <https://doi.org/10.1021/acsami.6b10898>.
- [11] H.-L. Yip, A.K.-Y. Jen, Recent advances in solution-processed interfacial materials for efficient and stable polymer solar cells, *Energy Environ. Sci.* 5 (2012) 5994–6011, <https://doi.org/10.1039/C2EE02806A>.
- [12] B. Usmani, R. Ranjan, Prateek, S.K. Gupta, R.K. Gupta, K.S. Nalwa, A. Garg, Inverted PTB7-Th:PC71BM organic solar cells with 11.8% PCE via incorporation of gold nanoparticles in ZnO electron transport layer, *Sol. Energy* 214 (2021) 220–230, <https://doi.org/10.1016/j.solener.2020.11.071>.
- [13] V.-H. Tran, R.B. Ambade, S.B. Ambade, S.-H. Lee, I.-H. Lee, Low-temperature solution-processed SnO₂ nanoparticles as a cathode buffer layer for inverted organic solar cells, *ACS Appl. Mater. Interfaces* 9 (2017) 1645–1653, <https://doi.org/10.1021/acsami.6b10857>.
- [14] H. Jin, M.D. Farrar, J.M. Ball, A. Dasgupta, P. Caprioglio, S. Narayanan, R.D. J. Oliver, F.M. Rombach, B.W.J. Putland, M.B. Johnston, H.J. Snaith, Alumina nanoparticle interfacial buffer layer for low-bandgap lead-tin perovskite solar cells, *Adv. Funct. Mater.* n/a (2023) 2303012, <https://doi.org/10.1002/adfm.202303012>.
- [15] L.S. Pali, J.K. Tiwari, N. Ali, S. Ghosh, K.S. Nalwa, A. Garg, Development of MoO₃/Au/MoO₃ top transparent conducting electrode for organic solar cells on opaque substrates, *Energy Technol.* 10 (2022) 2100689, <https://doi.org/10.1002/ente.202100689>.
- [16] H. Chen, Z. Yin, Y. Ma, D. Cai, Q. Zheng, Solution-processed polymer bilayer heterostructures as hole-transport layers for high-performance opaque and semitransparent organic solar cells, *Mater. Today Energy* 35 (2023) 101322, <https://doi.org/10.1016/j.mtener.2023.101322>.
- [17] M. Li, Y. Xie, R.F. Lin, Z. Li, S. Yang, A.K.-Y. Jen, Self-assembled monolayers as emerging hole-selective layers enable high-performance thin-film solar cells, *Innov.* 4 (2023), <https://doi.org/10.1016/j.xinn.2022.100369>.
- [18] T. Jiang, Y. Yang, X. Hao, J. Fan, L. Wu, W. Wang, G. Zeng, M.A. Halim, J. Zhang, Self-assembled monolayer hole transport layers for high-performance and stable inverted perovskite solar cells, *Energy Fuels* 38 (2024) 21371–21381, <https://doi.org/10.1021/acs.energyfuels.4c03889>.
- [19] P. Ding, D. Yang, S. Yang, Z. Ge, Stability of organic solar cells: toward commercial applications, *Chem. Soc. Rev.* 53 (2024) 2350–2387, <https://doi.org/10.1039/D3CS00492A>.
- [20] P.K. Kanti, D.J. K, J. Swapnalini, V. Vicki Wanatasanappan, Advancements and prospects of MXenes in emerging solar cell technologies, *Sol. Energy Mater. Sol. Cells* 285 (2025) 113540, <https://doi.org/10.1016/j.solmat.2025.113540>.
- [21] W. Wang, C. Zhan, Y. Li, S. Xiao, Efficient inverted PM6:Y6 solar cells with tuned lateral phase separation and vertical composition distribution via bis(5-chlorothiophen-2-yl)alkane additives, *Chem. Eng. J.* 466 (2023) 143289, <https://doi.org/10.1016/j.cej.2023.143289>.
- [22] Y. Yang, Y. Xiao, B. Xu, J. Hou, Cross-linkable cathode interlayer for inverted organic solar cells with enhanced efficiency and stability, *Adv. Energy Mater.* 13 (2023) 2301098, <https://doi.org/10.1002/aenm.202301098>.
- [23] L. Di Mario, D. Garcia Romero, H. Wang, E.K. Tekelenburg, S. Meems, T. Zaharia, G. Portale, M.A. Loi, Outstanding fill factor in inverted organic solar cells with SnO₂ by atomic layer deposition, *Adv. Mater.* n/a (2023) 2301404, <https://doi.org/10.1002/adma.202301404>.
- [24] S. Banerjee, S.K. Gupta, A. Singh, A. Garg, Buffer layers in inverted organic solar cells and their impact on the interface and device characteristics: an experimental and modeling analysis, *Org. Electron. Physics, Mater. Appl.* 37 (2016) 228–238, <https://doi.org/10.1016/j.orgel.2016.06.031>.
- [25] S.K. Gupta, A. Sharma, S. Banerjee, R. Gahlot, N. Aggarwal, Deepak, A. Garg, Understanding the role of thickness and morphology of the constituent layers on the performance of inverted organic solar cells, *Sol. Energy Mater. Sol. Cells* 116 (2013), <https://doi.org/10.1016/j.solmat.2013.03.027>.
- [26] E. Gutierrez-Partida, M. Rusu, F. Zu, M. Raoufi, J. Diekmann, N. Tokmoldin, J. Warby, D. Menzel, F. Lang, S. Shah, S. Shoaei, L. Korte, T. Unold, N. Koch, T. Kirchartz, D. Neher, M. Stolterfoht, Toward understanding the built-in field in perovskite solar cells through layer-by-layer surface photovoltage measurements, *ACS Appl. Mater. Interfaces* 17 (2025) 11176–11186, <https://doi.org/10.1021/acsami.4c14194>.
- [27] L. Cattin, G. Louarn, L. Arzel, N. Stephan, M. Morsli, J.C. Bernède, Power conversion efficiency improvement of planar organic photovoltaic cells using an original hybrid electron-transporting layer, *ACS Omega* 6 (2021) 6614–6622, <https://doi.org/10.1021/acsomega.0c05259>.
- [28] L. Caliò, B.R. Patil, J. Benduhn, K. Vandewal, H.-G. Rubahn, M. Madsen, S. Kazim, S. Ahmad, Benzothiadiazole-triphenylamine as an efficient exciton blocking layer in small molecule-based organic solar cells, *Sustain. Energy Fuels* 2 (2018) 2296–2302, <https://doi.org/10.1039/C8SE00251G>.
- [29] Z. You, A. Gao, Y. Liu, Interfacial modification in organic solar cells, *Chem. Commun.* (2025), <https://doi.org/10.1039/D4CC06507G>.
- [30] J. Hack, C. Luderer, C. Reichel, R. Opila, M. Bivour, Determining limitations of capacitance-voltage measurements of built-in voltage as an alternative to surface photovoltage for a-Si:H/c-Si heterojunctions, *Sol. Energy Mater. Sol. Cells* 219 (2021) 110794, <https://doi.org/10.1016/j.solmat.2020.110794>.
- [31] S.K. Gupta, L.S. Pali, A. Garg, Impedance spectroscopy on degradation analysis of polymer/fullerene solar cells, *Sol. Energy* 178 (2019) 133–141, <https://doi.org/10.1016/j.solener.2018.12.024>.
- [32] S.K. Gupta, J. Yadav, N. Chaturvedi, R. Ranjan, L.S. Pali, K.S. Nalwa, A. Garg, Role of DIO vis-à-vis microstructural kinetics during thermal annealing on the performance of PTB7:PC71BM organic solar cells, *Sol. Energy* 213 (2021) 27–35, <https://doi.org/10.1016/j.solener.2020.11.019>.
- [33] S.K. Gupta, D.C. Tripathi, A. Garg, S.K. Pathak, Determination of defect states and surface photovoltage in PTB7:PC71BM based bulk heterojunction solar cells, *Sol. Energy Mater. Sol. Cells* 224 (2021) 110994, <https://doi.org/10.1016/j.solmat.2021.110994>.
- [34] D.C. Tripathi, S.K. Gupta, A. Kumar, S.K. Pathak, A. Garg, Impact of recombination mechanisms on the capacitance-voltage characteristics in bulk heterojunction organic solar cells, *Synth. Met.* 297 (2023) 117419, <https://doi.org/10.1016/j.synthmet.2023.117419>.
- [35] B. Chen, X. Qiao, C.-M. Liu, C. Zhao, H.-C. Chen, K.-H. Wei, B. Hu, Effects of bulk and interfacial charge accumulation on fill factor in organic solar cells, *Appl. Phys. Lett.* 102 (2013) 193302, <https://doi.org/10.1063/1.4805053>.
- [36] S.K. Gupta, S. Banerjee, A. Singh, L.S. Pali, A. Garg, Modeling of degradation in normal and inverted OSC devices, *Sol. Energy Mater. Sol. Cells* 191 (2019), <https://doi.org/10.1016/j.solmat.2018.11.039>.
- [37] B. Ray, A.G. Baradwaj, B.W. Boudouris, M.A. Alam, Defect characterization in organic semiconductors by forward bias capacitance–voltage (FB-CV) analysis, *J. Phys. Chem. C* 118 (2014) 17461–17466, <https://doi.org/10.1021/jp505500r>.
- [38] U.K. Verma, S. Kumar, Y.N. Mohapatra, Measurement of contact surface photovoltage from forward bias C-V characteristics of P3HT:PCBM based BHJ solar cells, *Sol. Energy Mater. Sol. Cells* 172 (2017) 25–33, <https://doi.org/10.1016/j.solmat.2017.07.010>.
- [39] S.K. Gupta, L.S. Pali, A. Garg, Impedance spectroscopy on degradation analysis of polymer/fullerene solar cells, *Sol. Energy* 178 (2019), <https://doi.org/10.1016/j.solener.2018.12.024>.
- [40] S.L.M. van Mensvoort, R. Coehoorn, Determination of injection barriers in organic semiconductor devices from capacitance measurements, *Phys. Rev. Lett.* 100 (2008) 086802, <https://doi.org/10.1103/PhysRevLett.100.086802>.
- [41] D.C. Tripathi, Y.N. Mohapatra, Diffusive capacitance in space charge limited organic diodes: analysis of peak in capacitance–voltage characteristics, *Appl. Phys. Lett.* 102 (2013) 253303, <https://doi.org/10.1063/1.4812487>.
- [42] W.C. Germs, S.L.M. van Mensvoort, R.J. de Vries, R. Coehoorn, Effects of energetic disorder on the low-frequency differential capacitance of organic light-emitting diodes, *J. Appl. Phys.* 111 (2012) 074506, <https://doi.org/10.1063/1.3701575>.
- [43] T. Kirchartz, W. Gong, S.A. Hawks, T. Agostinelli, R.C.I. MacKenzie, Y. Yang, J. Nelson, Sensitivity of the mott-Schottky analysis in organic solar cells, *J. Phys. Chem. C* 116 (2012) 7672–7680, <https://doi.org/10.1021/jp300397f>.
- [44] M. Mingebach, C. Deibel, V. Dyakonov, Built-in potential and validity of the Mott-Schottky analysis in organic bulk heterojunction solar cells, *Phys. Rev. B* 84 (2011) 153201, <https://doi.org/10.1103/PhysRevB.84.153201>.
- [45] O. Oklobia, S. Komilian, T. Sadat-Shafai, Impedance spectroscopy and capacitance–voltage measurements analysis: impact of charge carrier lifetimes and mapping vertical segregation in bulk heterojunction P3HT:PCBM solar cells, *Org. Electron.* 61 (2018) 276–281, <https://doi.org/10.1016/j.orgel.2018.06.003>.
- [46] E. Regalado-Pérez, E.B. Díaz-Cruz, J. Villanueva-Cab, Impact of the hole transport layer on the space charge distribution and hysteresis in perovskite solar cells analysed by capacitance–voltage profiling, *Sustain. Energy Fuels* 9 (2025) 1225–1235, <https://doi.org/10.1039/D4SE01262C>.
- [47] M.Z. Iqbal, A. Bibi, S. Khan, S. Chandra, A. Kumar, S. Kaushal, V. Mishra, Y. S. Usmani, Enhancing charge extraction efficiency in PbS-I quantum dot solar cell through optimized interface engineering, *Sol. Energy* 287 (2025) 113249, <https://doi.org/10.1016/j.solener.2025.113249>.
- [48] Q. Niu, N.I. Crăciun, G.-J.A.H. Wetzaelaer, P.W.M. Blom, Origin of negative capacitance in bipolar organic diodes, *Phys. Rev. Lett.* 120 (2018) 116602, <https://doi.org/10.1103/PhysRevLett.120.116602>.
- [49] S. Kumar, U.K. Verma, Y.N. Mohapatra, Negative contribution to the reverse bias capacitance of organic diodes due to field dependent mobility: determination of barrier height and transport parameters, *J. Appl. Phys.* 124 (2018) 035501, <https://doi.org/10.1063/1.5026479>.
- [50] K.-G. Lim, H.-B. Kim, J. Jeong, H. Kim, J.Y. Kim, T.-W. Lee, Boosting the power conversion efficiency of perovskite solar cells using self-organized polymeric hole

- extraction layers with high work function, *Adv. Mater.* 26 (2014) 6461–6466, <https://doi.org/10.1002/adma.201401775>.
- [51] S. Züfle, M.T. Neukom, S. Altazin, M. Zinggeler, M. Chrapa, T. Offermans, B. Ruhstaller, An effective area approach to model lateral degradation in organic solar cells, *Adv. Energy Mater.* 5 (2015) 1500835, <https://doi.org/10.1002/aenm.201500835>.
- [52] S. Cho, K.-D. Kim, J. Heo, J.Y. Lee, G. Cha, B.Y. Seo, Y.D. Kim, Y.S. Kim, S. Choi, D. C. Lim, Role of additional PCBM layer between ZnO and photoactive layers in inverted bulk-heterojunction solar cells, *Sci. Rep.* 4 (2014) 4306, <https://doi.org/10.1038/srep04306>.
- [53] M. Ahmadi, Y.-C. Hsiao, T. Wu, Q. Liu, W. Qin, B. Hu, Effect of photogenerated dipoles in the hole transport layer on photovoltaic performance of organic-inorganic perovskite solar cells, *Adv. Energy Mater.* 7 (2017) 1601575, <https://doi.org/10.1002/aenm.201601575>.
- [54] N. Yao, J. Wang, Z. Chen, Q. Bian, Y. Xia, R. Zhang, J. Zhang, L. Qin, H. Zhu, Y. Zhang, F. Zhang, Efficient charge transport enables high efficiency in dilute donor organic solar cells, *J. Phys. Chem. Lett.* 12 (2021) 5039–5044, <https://doi.org/10.1021/acs.jpclett.1c01219>.
- [55] S. Liu, Z. Xue, Z. Liang, B. Zhao, W. Wang, Z. Cong, H. Wu, G. Lu, J. Zheng, C. Gao, High-performance PM6:Y6-based ternary solar cells with enhanced open circuit voltage and balanced mobilities via doping a wide-band-gap amorphous acceptor, *ACS Appl. Mater. Interfaces* 16 (2024) 36705–36714, <https://doi.org/10.1021/acsami.4c06326>.
- [56] C. Wöpke, C. Göhler, M. Saladina, X. Du, L. Nian, C. Greve, C. Zhu, K.M. Yallum, Y. J. Hofstetter, D. Becker-Koch, N. Li, T. Heumüller, I. Milekhin, D.R.T. Zahn, C. J. Brabec, N. Banerji, Y. Vaynzof, E.M. Herzog, R.C.I. MacKenzie, C. Deibel, Traps and transport resistance are the next frontiers for stable non-fullerene acceptor solar cells, *Nat. Commun.* 13 (2022) 3786, <https://doi.org/10.1038/s41467-022-31326-z>.
- [57] U.K. Verma, D.C. Tripathi, Y.N. Mohapatra, Direct determination of defect density of states in organic bulk heterojunction solar cells, *Appl. Phys. Lett.* 109 (2016) 113301, <https://doi.org/10.1063/1.4962827>.
- [58] L. Barnea-Nehoshtan, S. Kirmayer, E. Edri, G. Hodes, D. Cahen, Surface photovoltage spectroscopy study of organo-lead perovskite solar cells, *J. Phys. Chem. Lett.* 5 (2014) 2408–2413, <https://doi.org/10.1021/jz501163r>.
- [59] J.C. Wang, X.C. Ren, S.Q. Shi, C.W. Leung, P.K.L. Chan, Charge accumulation induced S-shape J-V curves in bilayer heterojunction organic solar cells, *Org. Electron.* 12 (2011) 880–885, <https://doi.org/10.1016/j.orgel.2011.02.016>.
- [60] S. Biring, Y.-M. Sung, T.P. Nguyen, Y.-Z. Li, C.-C. Lee, A.H. Yi Chan, B. Pal, S. Sen, S.-W. Liu, K.-T. Wong, Reconciling the value of Schottky barriers in small molecular organic photovoltaics from J-V and C-V measurements at low temperatures towards the estimation of open circuit voltage at 0 K, *Org. Electron.* 73 (2019) 166–171, <https://doi.org/10.1016/j.orgel.2019.06.014>.
- [61] I.C. Ghosekar, G.C. Patil, Review on performance analysis of P3HT:PCBM-based bulk heterojunction organic solar cells, *Semicond. Sci. Technol.* 36 (2021) 45005, <https://doi.org/10.1088/1361-6641/abe21b>.
- [62] M. Abdallaoui, N. Sengouga, A. Chala, A.F. Meftah, A.M. Meftah, Comparative study of conventional and inverted P3HT: PCBM organic solar cell, *Opt. Mater.* 105 (2020) 109916, <https://doi.org/10.1016/j.optmat.2020.109916>.
- [63] C. Zhao, B. Chen, X. Qiao, L. Luan, K. Lu, B. Hu, Revealing underlying processes involved in light soaking effects and hysteresis phenomena in perovskite solar cells, *Adv. Energy Mater.* 5 (2015) 1500279, <https://doi.org/10.1002/aenm.201500279>.
- [64] V. V Brus, A.K.K. Kyaw, P.D. Maryanchuk, J. Zhang, Quantifying interface states and bulk defects in high-efficiency solution-processed small-molecule solar cells by impedance and capacitance characteristics, *Prog. Photovoltaics Res. Appl.* 23 (2015) 1526–1535, <https://doi.org/10.1002/pip.2586>.
- [65] T. Wu, L. Collins, J. Zhang, P.-Y. Lin, M. Ahmadi, S. Jesse, B. Hu, Photoinduced bulk polarization and its effects on photovoltaic actions in perovskite solar cells, *ACS Nano* 11 (2017) 11542–11549, <https://doi.org/10.1021/acsnano.7b06413>.